Available online at www.sciencedirect.com
SCIENCE DIRECT®
Nuclear Instruments and Methods in Physics Research A 507 (2003) 609–616
NUCLEAR INSTRUMENTS & METHODS IN PHYSICS RESEARCH Section A
www.elsevier.com/locate/nima

The LUNA II 400 kV accelerator ☆

A. Formicola[a], G. Imbriani[b,*], M. Junker[c], D. Bemmerer[d], R. Bonetti[f], C. Broggini[e], C. Casella[f], P. Corvisiero[g], H. Costantini[g], G. Gervino[h], C. Gustavino[c], A. Lemut[g], P. Prati[g], V. Roca[i], C. Rolfs[a], M. Romano[i], D. Schürmann[a], F. Strieder[a], F. Terrasi[j], H.-P. Trautvetter[a], S. Zavatarelli[g]

[a] *Institut für Physik mit Ionenstrahlen, Ruhr-Universität Bochum, Germany*
[b] *Osservatorio Astronomico Collurania, Teramo and INFN sez. Napoli, Italy*
[c] *Laboratori Nazionali del Gran Sasso dell INFN, Assergi, Italy*
[d] *Fachbereich Physik, Technische-Universität Berlin, Germany*
[e] *INFN, Padova, Italy*
[f] *Universitá di Milano, Dipartimento Di Fisica and INFN, Milano, Italy*
[g] *Universitá di Genova, Dipartimento di Fisica and INFN, Genova, Italy*
[h] *Universitá di Torino, Dipartimento di Fisica Sperimentale and INFN, Torino, Italy*
[i] *Universitá di Napoli, Dipartimento di Fisica and INFN, Napoli, Italy*
[j] *Seconda Universitá di Napoli, Dipartimento di Scienze Ambientali, Caserta and INFN, Napoli, Italy*

Received 1 April 2003; accepted 4 April 2003

Abstract

A second high current accelerator of 400 kV has been installed at the underground laboratory of Gran Sasso, called LUNA II. We describe this new facility as well as measurements of the proton beam characteristics: absolute energy, energy spread, and long-term energy stability. The absolute energy was determined to a precision of ± 300 eV at $E_p = 130$–400 keV using the energy of the capture γ-ray transition of $^{12}C(p,\gamma)^{13}N$ as well as resonance energies at $E_p = 309$–389 keV of $^{23}Na(p,\gamma)^{24}Mg$, $^{26}Mg(p,\gamma)^{27}Al$, and $^{25}Mg(p,\gamma)^{26}Al$. The resonance studies led to a proton energy spread of better than 100 eV and a long-term energy stability of 5 eV per hour.

PACS: 29.17.+w; 26

Keywords: Electrostatic accelerator; Calibration; Nuclear astrophysics

1. Introduction

A second high current accelerator of 400 kV has been installed at the underground laboratory of Gran Sasso (Italy), called LUNA II (LUNA = Laboratory Underground for Nuclear Astrophysics). It complements LUNA I [1] a

☆ Supported in part by INFN, GSI (Bo-Rol 125/2) and BMBF (05CL1PC1-1).

*Corresponding author. Address for correspondence: Instituto Nazionale di Fisica Nucleare Sezione di Napoli, Complesso Universitario di Monte Sant'Angelo, Via Cintia ed. G, 80126 Naples, Italy. Fax: +39081676346.

E-mail address: gianluca.imbriani@na.infn.it (G. Imbriani).

0168-9002/03/$ - see front matter © 2003 Elsevier Science B.V. All rights reserved.
doi:10.1016/S0168-9002(03)01435-9

50 kV accelerator facility at Gran Sasso, towards higher energies. Similarly as LUNA I, LUNA II is dedicated to measure the cross section $\sigma(E)$ of charged-particle-induced nuclear reactions of astrophysical interest (e.g. hydrogen burning in the sun) at energies far below the respective Coulomb barrier and possibly close or within the associated Gamow energy E_G. For example, the $^{14}N(p,\gamma)^{15}O$ reaction, the slowest reaction in the CNO-cycle, was measured previously via γ-ray spectroscopy only down to $E_p \cong 250$ keV, while $E_G = 28$ keV in the sun.

Due to the nearly exponential drop of $\sigma(E)$ with decreasing energy E, the absolute incident energy E needs to be known with high accuracy. For the above reaction, an error of 1.5 keV in beam energy at 100 keV leads to an error in $\sigma(E)$ of about 20%. For similar reasons, the absolute energy spread and long-term energy stability must be known sufficiently well, where the latter feature is particularly important in view of the long running times (several days) at low energies.

In one set of experiments, the absolute proton energy at $E_p = 130$–400 keV was determined from the energy of the capture γ-ray transition in $^{12}C(p,\gamma)^{13}N$ [2]. The results have been checked using (p,γ) resonances on ^{23}Na, ^{25}Mg, and ^{26}Mg. These resonances were also used to measure the energy spread ΔE_B and the long-term energy stability of the proton beam.

2. Experimental equipment

2.1. Accelerator

Luna II involves a 400 kV electrostatic accelerator (High Voltage Engineering Europe, Netherlands) imbedded in a tank, which is filled with a gas mixture N_2/CO_2 at 20 bar. The high voltage (HV) is generated by an Inline-Cockcroft-Walton power supply (located inside the tank) capable to handle 1 mA at 400 kV; its DC input is provided by a low-ripple power supply rating at maximum 300 V and 10 A. The HV at the terminal (ion source) is filtered by a stabilization system consisting of a RC-filter located at the output of the HV power supply and an active feedback loop based on a chain of resistors which measure the HV at the terminal. The resistors have an accuracy of 0.1% and a temperature coefficient of ≤ 10 ppm/°C. The system reduces the HV-ripple to 30 Vpp for frequencies larger than 1 Hz; the ripple is monitored with a pick-up plate. The system is expected to have a reproducibility and long-term stability of the HV of 20 Vpp at 400 kV over several days, consistent with observation (see below).

The radio-frequency ion source provides ion beams of 1 mA hydrogen ($75\%H^+$) and 500 μA He^+ over a continuous operating time of about 40 days. The ion source is mounted directly on the accelerator tube. The ions are extracted by an electrode, which is part of the accelerator tube, and its voltage is thus included in the overall HV at the terminal. The accelerator tube is equipped with an adjustable shortening rod and a magnetic X-ray suppression system. With a 5 mm thick Pb shield around the tank, the radiation level in the control room is below 0.5 mSv/h for the above ion beams at 400 kV.

With a 45° magnet (30 cm radius, 3 cm gap, 1.6 MeV amu; 1×10^{-4} stability/h) and a vertical steerer located before the magnet, the ion beam is guided and focused properly to the target station. In the energy range of 150–400 keV, the proton beam current on target is typically 500 μA, with a half-angle divergence of 0.3°; at 50 keV, the proton current is about 150 μA.

The accelerator, the experimental equipment, and the data handling is controlled by a PLC-based computer, which allows for a safe operation over long periods of running time without the constant presence of an operator on site.

2.2. Targets

The ^{12}C targets (natural isotopic composition) were obtained by cutting 1 mm thick slices of a pure graphite rod. They were then pressed on a directly water cooled Cu backing and could withstand up to 500 μA beam current over periods of several days. The Mg targets were produced by reducing MgO powder (natural Mg and isotopically enriched ^{25}Mg) in a Ta boat. The resulting Mg-films with a typical thickness of 50 $\mu g/cm^2$ were deposited on Ta backings, which were

directly water cooled. The Na targets were made by evaporating NaCl (thickness 50 μg/cm^2) on a Ta backing. The targets were stored and transported under Ar atmosphere to minimize surface oxidation. All targets had a diameter of 25 mm and were mounted in a set-up shown in Fig. 1. The proton beam passed through a $\ell = 30$ cm long Cu tube (diameter $\varnothing = 30$ mm), a rectangular collimator (18×18 mm^2), and a cold trap ($\ell = 45$ mm, $\varnothing = 28$ mm) extending to within 2 mm from the target, where the target plane was oriented perpendicularly to the beam direction. The Cu tube and the cold trap were both cooled to liquid nitrogen temperature. With a turbo pump installed below the Cu tube, the arrangement led to a pressure in the target chamber of 5×10^{-7} mb, whereby no C deposition was observed on the targets. A voltage of minus 300 V was applied to the cold trap to minimize emission of secondary electrons from both the target and the collimator; the precision in the current integration was estimated to be about 3%. The beam profile on the target could be visually inspected through a window on the 125° port of the target chamber. The profile was also controlled by sweeping the beam in the x and y directions within the geometry of the collimator.

2.3. Detector and electronics

A High Purity (HP) Ge-detector with 120% efficiency (compared to a $3'' \times 3''$ NaI crystal) was placed at 0° with respect to the beam axis at a distance $d = 39$ mm from the target (see Fig. 1). The observed energy resolution was $\Delta E_\gamma = 2.2$ keV at $E_\gamma = 1.33$ MeV. Standard electronics was used for processing the detector pulses which were finally stored in a 16k ADC. The acquisition unit was placed close to the experiment and the processed digitized data were send via Ethernet to a PC for analysis. In this way, problems due to ground loops could be avoided.

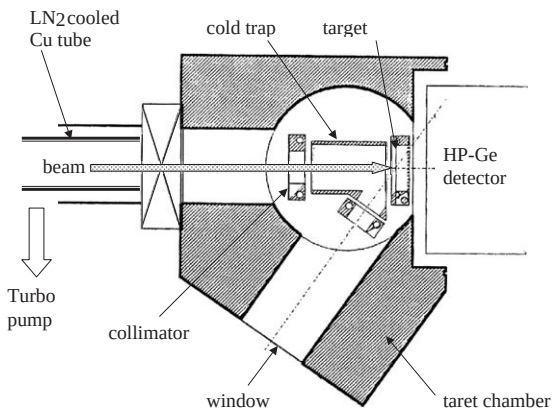

Fig. 1. Schematic diagram of the experimental set-up (for details, see text).

3. Experimental procedures

3.1. Resonance studies

The absolute energy E and the energy spread ΔE_B of the proton beam have been measured at (p, γ) resonances of ^{25}Mg, ^{26}Mg, and ^{23}Na, whose parameters are given in Table 1 together with the expected Doppler broadening ΔE_D at 300 K [3]. In these measurements the accelerator beam energy was chosen about 1 keV above E_R and the actual energy on the target was reduced by applying a positive voltage up to 3 kV on target. A program was written with LabView which controlled the voltage stepping and simultaneous recording of characteristic counting rates from the Ge detector.

In Fig. 2 an example is shown for the $E_p = 389$ keV resonance of the reaction ^{25}Mg(p, γ)^{26}Al. The voltage was varied between 900 and 1400 V in steps of 10 V of 60 s duration each. The γ-ray yield was recorded above $E_\gamma = 2.8$ MeV. Due to the slowing down of the protons the yield shows a characteristic resonance drop at high voltage of the accelerator minus the bias voltage when reaching the resonance energy E_R. The increase of the yield from the thick target yield plateau before the steep drop is due to the Lewis effect [8] and can only be seen for a low spread ΔE_B of the proton beam. This effect is due to the fact that the first layer of the target "sees" an un-degraded proton energy distribution = energy resolution. This distribution of width ΔE_B has been fitted in first approximation with an individual Gaussian (dotted curve in Fig. 2) followed by an error function to represent the thick target yield (dashed curve in Fig. 2), which includes ΔE_D, and ΔE_B.

Table 1
Resonance parameters

Reaction	Resonance energy E_R (keV)	Resonance width Γ (eV)	Doppler broadening ΔE_D (eV)	Beam spread ΔE_B (eV)	HV + PV (kV)	Shift (keV)
^{23}Na(p, γ)^{24}Mg	308.75 ± 0.06[a]	< 36[a]	58[a]	71	311.24	2.49 ± 0.06
^{25}Mg(p, γ)^{26}Al	316.11 ± 0.11[b]	< 37[a]	58[a]	120	318.83	2.65 ± 0.11
^{26}Mg(p, γ)^{27}Al	338.30 ± 0.10[c]	< 40[a]	59[a]	101	340.80	2.50 ± 0.10
^{25}Mg(p, γ)^{26}Al	389.24 ± 0.11[b]	< 4[d]	62[a]	72	392.17	2.93 ± 0.11

[a] Ref. [3].
[b] Ref. [4].
[c] Weighted average of values from Refs. [5,6].
[d] Ref. [7].

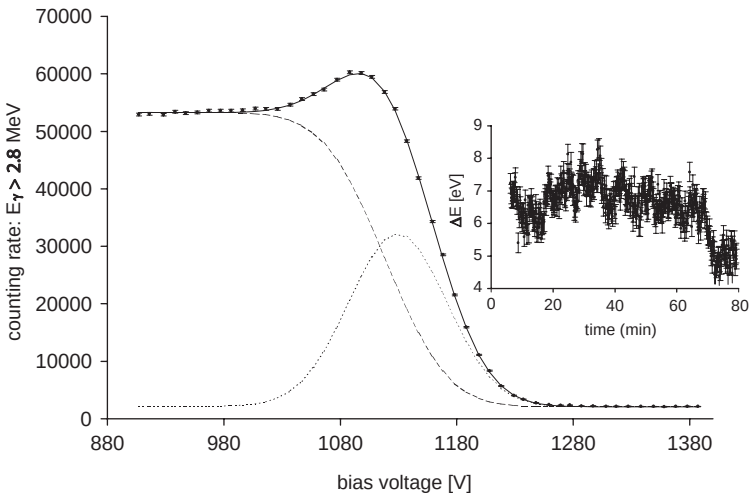

Fig. 2. Thick-target yield curve of the $E_R = 389$ keV resonance in ^{25}Mg(p, γ)^{26}Al obtained by varying a bias voltage applied to the target. The dotted curve represents the energy distribution of the incoming proton beam and the dashed curve represents an error function for the thick-target yield curve. The solid curve is the convolution of the dotted and dashed curves leading to the "*Lewis*" peak. The insert shows the yield variation at the 50% yield point as a function of time, where the yield variation was translated into an energy variation ΔE.

The solid curve in Fig. 2 represents the sum of the two functions. From Table 1 it can be seen that the resonance width Γ is much smaller than the deduced beam spread. The resonance is observed at HV + PV = 392.17 kV (HV and PV being the high voltage of the accelerator and the probe voltage of the ion source, respectively (Section 3.3), while $E_p = 389.24$ keV [4]. Hence, a shift of 2.93 keV must be taken into account in the energy determination (Table 1). The Gaussian and error functions have a total width of FWHM = 98 eV. Subtracting quadratically the Doppler broadening of 62 eV (Table 1) one obtains a beam spread of 72 eV at $E_p = 390$ keV. The ΔE_B values and shifts obtained for the other resonances are given in Table 1, obtained at different times, which led to $\Delta E_B \leqslant 100$ eV. The observed shift in the resonance energy is compared in Fig. 7 with the shift values deduced from ^{12}C(p, γ)^{13}N.

Due to the steep slope of the yield curve in Fig. 2 near the resonance energy (50% yield point) one can monitor sensitively the long-term energy

stability of the accelerator: a change in yield at the midpoint by 20% corresponds to an energy shift of 10 eV. The inset diagram of Fig. 2 shows this variation in units of eV. The step duration was 10 s over a period of 73 min: shifts of only ± 2 eV were recorded during that time.

3.2. Studies of $^{12}C(p,\gamma)^{13}N$

The $^{12}C(p,\gamma)^{13}N$ reaction has been used as an alternative method to determine the absolute proton energy over a wide energy range. An advantage in using carbon as target was that the results are not influenced by any C-deposition on the target during the runs. The expected γ-ray energy from $^{12}C(p,\gamma)^{13}N$ for a thin target is $E_\gamma = Q + E_{cm}$ with $Q = 1943.5 \pm 0.3$ keV [9] and ranges from $E_\gamma = 2036$ to 2313 keV for $E_p = 100$–400 keV, respectively. Accurate calibration lines from γ-ray sources can be found in the literature for this energy range. The energy calibration of the γ-ray spectra has been checked at various times and was found to be stable within ± 100 eV over several weeks. In addition, the calibration was monitored during each run and corrections have been made when necessary. In this way, the calibration error could be kept below 50 eV.

In the present work the 1 mm thick graphite target can be considered infinitely thick for all proton energies used. Even moderate target sputtering will not change this condition and will therefore also not influence the extraction of the γ-ray energy.

In order to determine the beam energy from the observed γ-ray energy we studied in detail the expected line shape. This shape is influenced by several parameters:

- The energy loss of the protons in the infinitely thick target gives rise to a drop in counting rate at the low energy tail of the capture line according to the known drop in cross section of the $^{12}C(p,\gamma)^{13}N$ reaction [10]: $\sigma(E_p)$.
- The stopping power of the protons in carbon is a function of proton energy [11]: $dE/dx(E_p)$.
- The position of the high energy rise of the γ-ray line is influenced by the Doppler effect and the recoil of the compound nucleus ($= 0.5E_\gamma^2/Mc^2 \cong 0.3$ keV).
- An asymmetry in the peak shape can be expected due to the relatively large solid angle of the detector at a distance of $d = 39$ mm from the target which gives rise to a change in the Doppler shift.

If only the first two aspects are taken into account, the number of counts in channel i, N_i, corresponding to the energy bin $E_{\gamma i}$ to $E_{\gamma i} + \delta E_\gamma$ (δE = dispersion in units of keV per channel) is given by the expression

$$N_i \propto \frac{\sigma(E_{pi})\delta E_\gamma \epsilon(E_{\gamma i})}{\frac{dE}{dx}(E_{pi})} \quad (1)$$

for $E_{pi} \leqslant E_p$ (E_p = incident proton energy), where $\varepsilon(E_{\gamma i})$ is the γ-ray detection efficiency. The result must be folded with the detector resolution ΔE_γ to obtain the experimental line shape. The conversion from $E_{\gamma i}$ to E_{pi} must finally include the Doppler and recoil effects, i.e. the last two aspects.

The influence of the Doppler effect on the position and line shape has been studied by a GEANT simulation [12], which included the detector geometry and the experimental dispersion. For $E_p = 400$ keV, $d = 20$ mm, and $\Delta E_\gamma = 0$ the simulated γ-ray line shape (open points in Fig. 3) is asymmetric, where the low-energy tail arises from a reduced Doppler shift for angles larger than 0°. When this shape is folded with the actual detector resolution, $\Delta E_\gamma = 3$ keV, the maximum shifts towards lower energies (filled-points in Fig. 3). This shift can be taken into account in the analysis by introducing an attenuation factor Q_{DS} for the determination of the Doppler shift: $E_\gamma = E_{\gamma 0}(1 + Q_{DS}v/c)$, with $Q_{DS} \to 1$ for large distances. It turns out that the shape of the Gauss broadened line can be represented well by a Gaussian with an increase of about 20% in the FWHM, as demonstrated by the solid curve through the filled-points in Fig. 3.

The Q_{DS} values were calculated from GEANT simulated spectra generated for infinitively thick ^{12}C-targets and distances $d = 19$–104 mm in steps of 5 mm and for $d = 104$–234 mm (10 mm steps). These spectra were analysed with the function described below and compared with the calculated

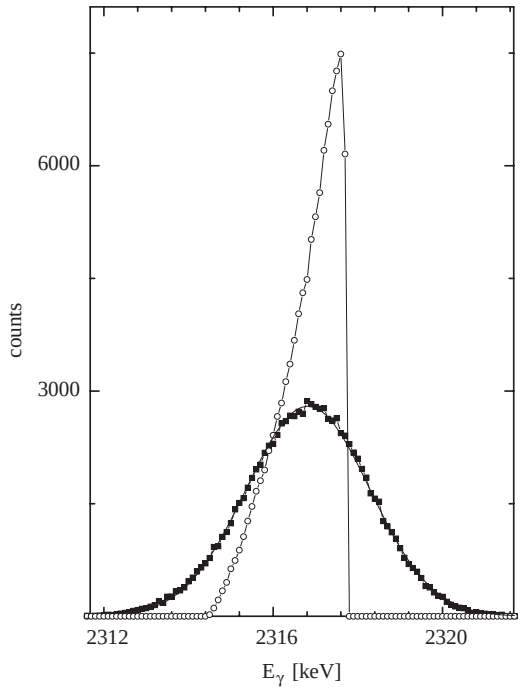

Fig. 3. The open-points represent the simulated Doppler effect near 0^0, i. e. the energy γ-ray distribution of $^{12}C(p,\gamma)^{13}N$ at $E_p = 400$ keV due to the finite size of the Ge-detector (distance of the detector to target = 20 mm). The results were folded with a 3 keV energy resolution of the detector leading to the filled-in points, which can be described well by a Gaussian distribution (solid curve through the filled-in-points).

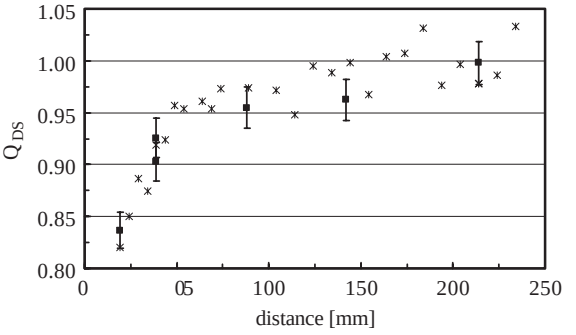

Fig. 4. Attenuation factor Q_{DS} of the Doppler shift for the capture transition in $^{12}C(p,\gamma)^{13}N$ at $E_p = 380$ keV as a function of distance between target and Ge-detector: crosses = GEANT simulations, filled-squares = experimental values normalized to 1.0 at 214 mm distance.

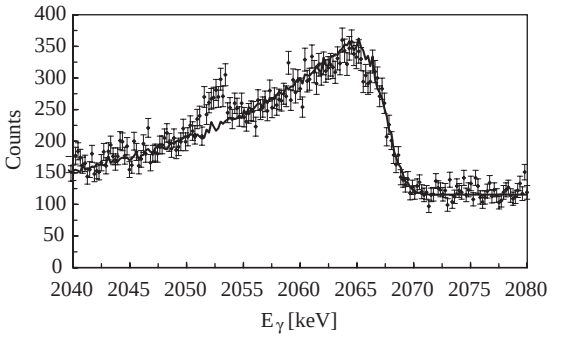

Fig. 5. Relevant section of the γ-ray spectrum near the capture line of $^{12}C(p,\gamma)^{13}N$ at the lowest proton energy, $E_p = 133$ keV. The solid curve through the data points represents a GEANT simulation.

full shift. The resulting Q_{DS} values are shown as crosses in Fig. 4.

Experimentally, we obtained spectra at $E_p = 380$ keV and $d = 19$–214 mm in 5 steps; the spectra were analysed as described above. The result for $d = 214$ mm was normalized to 1.0 on the basis of the GEANT results and the other Q_{DS} values (filled square points in Fig. 4) scaled accordingly. The agreement between simulation and observation is within experimental error. The result for $d = 39$ mm (distance in the calibration runs) is $Q_{DS} = 0.90 \pm 0.03$, where the error translates into a systematic error of ± 0.1 keV in the E_p determination.

A GEANT simulated spectrum at $E_p = 133$ keV is compared with the experimental line shape in Fig. 5, where the comparison involved an overall normalisation factor for the number of counts per channel and an energy shift; the resulting χ^2-value, $\chi^2 = 1.1$, demonstrates the validity of the GEANT simulation. Finally the spectrum obtained at each E_p value was fitted by a folding of Eq. (1) with the response function of the detector (i.e. a gaussian). The resulting fit, e.g. at $E_p = 350$ keV ($\chi^2 = 1.1$) is shown in Fig. 6. The fit function and the GEANT simulations yielded identical observed energy shifts Δ (Section 3.3).

3.3. Results

The energy calibration of the accelerator was obtained by determining the shift between the high voltage reading of the accelerator (HV) plus

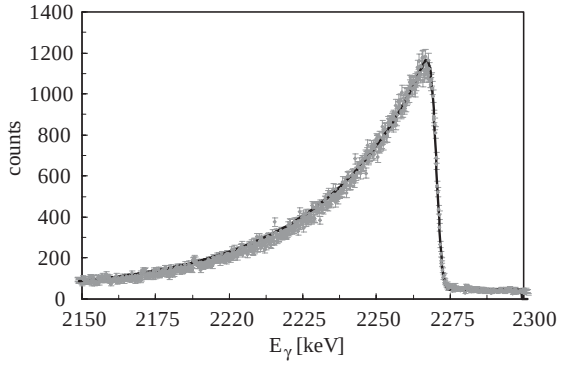

Fig. 6. Relevant section of the γ-ray spectrum near the capture line of $^{12}C(p,\gamma)^{13}N$ at $E_p = 350$ keV. The solid curve through the data points represents a fit to the data.

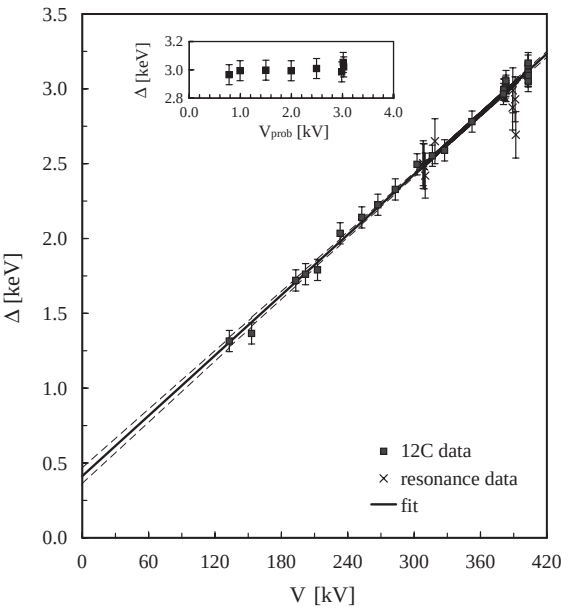

Fig. 7. From the readings of the high voltage (HV) and ion source probe voltage (PV) one expects a proton energy from the accelerator of $E_{ACC} = V = HV + PV$. The deviation of expected and observed proton energy leads to a shift Δ, which is shown as a function of V. The solid line assumes a linear dependence of Δ from V and the dashed lines represent the uncertainty band around Δ. The insert shows the dependence of the observed shift Δ on the probe voltage at $V = 380$ kV.

the probe voltage (PV) of the ion source and the position of the fit function, corrected for the Doppler shift and for the recoil effect. The results are shown in Fig. 7, where only the statistical errors arising from the energy calibration of the γ-spectrum and the uncertainty on the line-shape fit parameter are reported. An additional systematic uncertainty of 100 eV from Q_{DS} and the error on the reaction Q-value (± 300 eV) have to be included. The accelerator had to be opened for an ion source replacement between the runs in February 2002 and March 2002. Excellent agreement between the two data sets was found in the overlapping energy region: it illustrates, that the calibration does not depend on the source condition. The dependence of the calibration on the probe voltage of the ion source has been tested at $E_p = 380$ keV (inset of Fig. 7): no systematic change could be found within ± 25 eV. Included in Fig. 7 are also the results from the observation of resonances of Table 1 (crosses in Fig. 7) in the time period from September 2000 to February 2002. These results agree very well with the $^{12}C(p,\gamma)^{13}N$ reaction data and show again the long-term energy stability and reliability of the accelerator. The data in Fig. 7 suggest a linear function for the observed shift Δ versus $V = (HV + PV)$,

$$\Delta = m \cdot V + b \tag{2}$$

where $m = (0.0067 \pm 0.0002)$ keV/kV and $b = (0.41 \pm 0.05)$ keV. Thus,

$$E_p = m' \cdot V - b \tag{3}$$

where $m' = 1 - m = 0.9933$ keV/kV. The origin of the fit function has been chosen to be $V_0 = 328$ kV for a meaningful error estimation: thus

$$\Delta = m(V - V_0) + b' \tag{4}$$

with $m = (0.0067 \pm 0.0002)$ keV/kV and $b' = (2.61 \pm 0.05)$ keV. The dashed lines in Fig. 7 indicate the statistical uncertainty band which is of course larger outside the region of experiment. This error estimate is only valid for the assumption of a linear function between Δ and V. The error is smaller than 60 eV between $E_p = 100$ and 400 keV and is therefore of the same order as the systematical uncertainty of 100 eV from Q_{DS} and three times smaller then the error in the reaction Q-value (300 eV). For the example discussed in the introduction, this uncertainty amounts to a 5%

uncertainty in the cross section measurement of $^{14}N(p,\gamma)^{15}O$ at $E_p = 100$ keV.

Acknowledgements

We are grateful to P. Bezzon ed A. Lombardi of the Legnaro INFN National Laboratories for the valuable support in the set-up and operation of the accelerator. Two of the authors, G.I. and F.T., thank the Director of the Astronomical Observatory of Collurania, Prof. Amedeo Tornambé, for the support, and gratefully acknowledge Lucio Gialanella and Oscar Straniero for the fruitful discussions.

References

[1] U. Greife, et al., Nucl. Instr. and Meth. A 350 (1994) 327.
[2] T. Freye, H. Lorenz-Wirzba, B. Cleff, H.P. Trautvetter, C. Rolfs, Z. Phys. A 281 (1977) 211.
[3] M. Uhrmacher, K. Pampus, F.J. Bergmeister, D. Purschke, K.P. Lieb, Nucl. Instr. and Meth. B 9 (1985) 234.
[4] F.J. Bergmeister, K.P. Lieb, K. Pampus, M. Uhrmacher, Z. Phys. A 320 (1985) 693.
[5] P.M. Endt, Nucl. Phys. A 521 (1990) 1.
[6] L. Buchmann, H.W. Becker, K.U. Kettner, W.E. Kieser, P. Schmalbrock, C. Rolfs, Z. Phys. A 296 (1980) 273.
[7] A.E. Champagne, A.J. Howard, P.D. Parker, Nucl. Phys. A 402 (1983) 179.
[8] H.W. Lewis, Phys. Rev. 125 (1962) 937.
[9] F. Ajzenberg-Selove, Nucl. Phys. A 523 (1991) 1 National Nuclear Data Center of the Brookhaven National Laboratory, Upton, NY, USA (updated 1995).
[10] C. Rolfs, R.E. Azuma, Nucl. Phys. A 227 (1974) 291.
[11] H. Andersen, J.F. Ziegler, The Stopping and Ranges of Ions in Matter, Vol. 3, Pergamon, New York, 1977.
[12] GEANT4: An Object-Oriented Toolkit for Simulation in HEP, The RD44 Collaboration, CERN/LHCC 95-70, 1995 and The Geant4 Collaboration, http://wwwinfo.cern.ch/asd/geant4/geant4.html.